Biomedical Signal Processing and Control 54 (2019) 101630

Contents lists available at ScienceDirect

Biomedical Signal Processing and Control

journal homepage: www.elsevier.com/locate/bspc

On the existence of phase-synchronised states during motor imagery tasks

Lorena Santamaria[a,*], Christopher James[b]

[a] WMG, University of Warwick, Coventry, CV4 7AL, UK
[b] Warwick Engineering in Biomedicine, School of Engineering, University of Warwick, Coventry, CV4 7AL, UK

ARTICLE INFO

Article history:
Received 21 November 2018
Received in revised form 13 June 2019
Accepted 22 July 2019
Available online 1 August 2019

Keywords:
EEG
Clustering
Motor imagery tasks
Schematic emotional faces
Functional brain connectivity
Synchrostates

ABSTRACT

Phase synchronization as a mechanism to measure functional connectivity has been widely used in the literature. However, these studies largely assume that functional connectivity remains constant across a cognitive task and assesses the changes in connectivity across the whole block, hence losing the temporal evolution of phase synchrony. We applied a wavelet-based phase analysis on EEG data during the performance of two motor imagery tasks. This method showed the existence of a reduced number of unique phase-synchronised states during the performance of motor imagery tasks using novel stimuli; schematic faces showing different emotions ("emoticons"). For all participants, these states remained stable for a few milliseconds before switching to the next state following a well-defined sequence. This results demonstrate that the occurrence of these phase states and their temporal stability (switching patterns) are task specific indicating existence of different processing dynamics for the two motor imagery task when are lock to a stimulus. The novel proposed methodology of study the temporal dynamics of brain connectivity can be seen as new method to characterise the dynamics of the underlying cognitive process occurring specifically for each one of the motor tasks. Therefore, this method can be potentially used for brain computer interface purposes.

1. Introduction

Brain activation, integration of the different cerebral areas and the temporal evolution of their synchronization are fundamental tools for understanding how the human brain develops a cognitive task under a specific stimulus. This can be assessed by means of functional brain connectivity [1]. In order to calculate functional brain connectivity among temporal signals, an increased number of data samples, hence a higher temporal resolution, is needed to achieve a meaningful result. Under this premise, the use of fMRI signals is limited by their low temporal resolution (usually around 2 s) as neural activity produces fast changes in the order of milliseconds [2]. The high temporal resolution of the electroencephalogram (EEG) and magnetoencephalogram (MEG) and their ability to record rapid neural activity makes them more suitable for measuring brain synchronization.

In the 1960s brain connectivity began to be measured by using cross correlation of pairs of EEG signals, introducing the concept of coherence [3]. This methodology is used to measure spatial correlations between signals over individual frequency bands (alpha, beta and gamma bands) during the performance of different motor tasks [4,5]. Coherence is sensitive to changes in power and in phase, mixing both effects when the cross-correlation between a pair of EEG channels is calculated [6,7]. There are several measures of phase synchronization, such as mutual information, coherence or cross-correlation, obtaining different performance levels but showing the same tendency in the synchronization levels [8]. However, no one of these techniques preserves information about the temporal evolution of the phase synchronization. On the other hand, methods based on the Wavelet transform allow estimation of phase synchronization whilst maintaining information relative to both phase and time evolution [9]. It is for these reasons this study performs an analysis of the temporal dynamics for phase synchronization in a Motor Imagery (MI) task.

Despite the growing use of functional brain connectivity as a mechanism to understand brain function and cerebrally activated areas, few studies exist that analyse the phase synchrony patterns under an MI task execution [2,10,11]. However, these few studies are focused on predefined states of a task, based on short frequency

* Corresponding author.
E-mail addresses: santamaria.L@warwick.ac.uk, santamariacovarrubiasL@cardiff.ac.uk (L. Santamaria), c.james@warwick.ac.uk (C. James).

https://doi.org/10.1016/j.bspc.2019.101630
1746-8094/

ranges or a small number of EEG channels. To address properly possible volume conduction effects and to exploit all the properties of connectivity measures is important to not confine the analysis to a subset of electrodes and consider different frequency bands.

Additionally, several studies related to resting state [12–15] have mentioned the idea of microstates based on the observation that the potential distribution maps remained stable during time intervals of the order of milliseconds. In the same respect in [9], they mention the concept of synchrostates after detecting stability periods when they observed the cross-channel phase difference.

In this study, the combination of connectivity metrics and the concept of microstates is used to pursue the identification of new biomarkers for a MI tasks classification problem. The main aims of this paper are: (1) validity of using "emoticons" as novel stimuli for motor imagery based tasks, (2) explore the existence of synchrostates in the two most typically used frequency bands for MI studies (α, β bands), (3) systematically explore the use of connectivity metrics from the phase-synchronized states as possible biomarkers to feed brain computer interface systems (BCI). The selection of schematic emotional faces has been done based on previous findings where had been demonstrated that emotional face stimuli lead to a stronger response across participants [16].

Furthermore, connectivity metrics from these stable states were calculated in order to quantitatively measure the differences between them. The use of graph theory-based metrics to investigate the underlying mechanisms of the brain provides a new dimension at different granularity levels and can be the key to stablish more standardised and reliable motor-imagery based BCI systems.

The rest of the paper is organized as follows. Section 2 describes the methodology followed to record the EEG signals. Section 3 explains the theoretical fundamentals of the procedure adopted to study brain connectivity patterns. Section 4 and 5 present the results and discussions respectively. Section 6 presents a summary of the achievements and future work followed by acknowledgements and references.

2. Experimental protocol

The dataset is collected from 10 participants (8 males) recruited by means of public announcements across the university campus. No selection criteria were applied during the process, all participants reported not being under any medication that could affect their performance. All the experiments were undertaken with the consent of each participant in accordance with the University of Warwick Ethical Committee, who approved the study (*REGO-2014-821*).

Participants were asked to perform two different imagined motor tasks accordingly to the emotions showed by the different schematic faces (emoticons) appearing in the screen. Happy faces are linked to the imagined movement of the right hand (*Thinking R* condition) and sad faces with the imagined movement of the left hand (*Thinking L* condition). A more detailed explanation of the experimental protocol can be found in [17]. Fig. 1 shows the complete block sequence of the experimental protocol. The tasks were divided in 4 blocks of 78 trials each with equal number of happy and sad faces.

Data were acquired at a 256 Hz sampling frequency using 64 channel cap with 62 active ring electrodes (sintered Ag/AgCl) covering the participant's scalp, plus two reference placed on the earlobes [18]. All of them are connected to a biosignal amplifier g.HIamp. Artefact free trials were divided into epochs for each condition: happy and sad emotions. The epoch duration is 1 s, starting at 100 ms before the target stimulus onset until 900 ms afterwards (providing 256 samples per EEG trial). The length of the epoch was selected as the one enhanced the maximum differences between classes for this specific methodology and to reduce the computational cost.

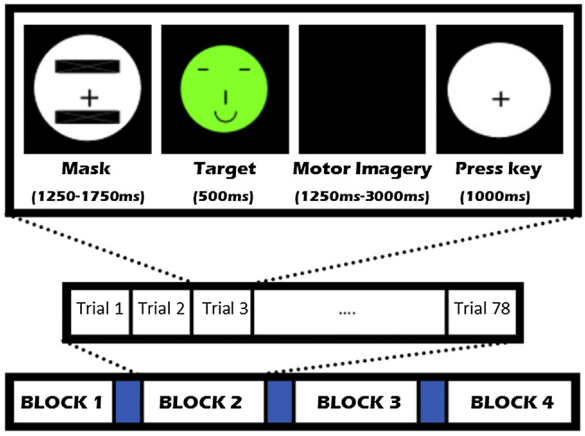

Fig. 1. Experimental sequence. Top row is a typical trial timing scheme: (1) masked faces lasting randomly between 1.25 s to1.75 s, (2) target stimuli illustrated by a green emoticon showing happiness or sadness (50% of probability, counterbalance across trials) lasting 0.5 s on the screen, (3) black background is presented from 1.25 s to 3 s to indicate to the participants the starting of the imagery task in accordance with the target stimulus, (4) black cross appearing for 1 s indicates the end of the trial. The complete experiment was divided into four blocks (last row) of 78 trials each (middle row). (For interpretation of the references to colour in this figure legend, the reader is referred to the web version of this article.)

3. Theoretical background

This section describes some of the concepts involved in the algorithm for analysing the temporal evolution of the brain connectivity during a MI task. This algorithm was firstly developed by Jamal et al. [19] during the study of autism spectrum disorder. In Section 3.1 the methodology used to determine the instantaneous difference of phase across electrodes is explained. The clustering algorithm is resented in Section 3.2. To conclude, the results of the clustering are translated into complex brain networks explained in Section 3.3.

3.1. Instantaneous phase difference

In order to measure the synchronization between two signals, $x(t)$ and $y(t)$, it is necessary to calculate the instantaneous phase for each one of these signals. With this aim the continuous complex wavelet transform (CWT) was applied to the dataset. The result of conducting a wavelet transform on a given signal is a complex matrix $WT_x(s,t)$ defined by a set of scales s and time t.

Afterwards, the instantaneous phase difference can be calculated as the difference of the complex arguments of the wavelet transforms $WT_x(s,t)$ and $WT_y(s,t)$ of the signals $x(t)$ and $y(t)$ as indicated by (1) [8,15].

$$\Delta\emptyset_{xy}(s,t) = \left|\emptyset_x(s,t) - \emptyset_y(s,t)\right|, \; where\, \emptyset_i(s,t) = \tan^{-1}\left(\frac{Im(WT_i)(s,t)}{Re(WT_i)(s,)}\right). \quad (1)$$

This procedure is repeated for each EEG channel, time sample, trial and scale (i.e. frequency) leading to a set of square matrices which are symmetrical and whose main diagonal is composed of zeros as it represents the instantaneous phase difference of an electrode with itself. Typically, EEG based MI research is focused in two frequency bands: α (8–13 Hz), β (13–30 Hz) [20]. The difference of phase for each pair of electrodes was averaged to obtain a frequency band specific $\Delta\emptyset^b_{x,y}(t)$ for each one of these bands. In the same way

Table 1
Pseudo code for the k-means clustering algorithm used to find the appropriated number of synchrostates for each condition and frequency band.

k-means clustering algorithm
1. Select number of clusters range m
2. Repeat for each m_i
• Repeat for each n_i
- Random initialization of initial centroids
- Form clusters by assigning each point to its closest centroid (cost function $J(\theta,U)$)
- Re-compute the centroids
• Repeat until convergence criterion is met
• Select and storage the minima of $J(\theta,U)$
3. Plot $J(\theta,U)$ versus m
4. Select m_i value showing the most significant "knee"

the resulting matrices, were averaged across trials for each one of the time samples [19]. It is well known that phase is circular in nature, consequently the difference of phase will be equally circular. To avoid this issue, firstly it is verified that the phase obtained from the CWT always remains between [-π, π]. In addition, the phase difference is normalized by using the maximum and minimum values of the dataset so the transformed data matrix values lie between [0,1] for each one of the time samples as described in [19].

3.2. Clustering

To discover significant patterns or features in the phase synchronization data obtained using the algorithm described in the previous section, an unsupervised learning algorithm is needed. In this case, the *k*-means clustering algorithm [21] is used. This is one of the most widely adopted approaches to unsupervised clustering. The methodology essentially involves the partitioning of the data space into *k* prototypes. Assuming that the number of clusters underlying X is known, and iteratively minimizes a cost function based on the Euclidian distance as a dissimilarity measure as shown in Eq. (2).

$$J\left(\theta, U\right) = \sum_{i=1}^{N}\sum_{j=1}^{m} u_{ij}\left\|X_i - \theta_j\right\|^2, \tag{2}$$

where $\theta = \left[\theta_1^T, \theta_2^T, \ldots, \theta_m^T\right]^T$ are the prototypes or centroids, $\|*\|$ expresses the Euclidean distance, θ_j is the mean vector of the j^{th} cluster, and $u_{ij} = 1$ if X_i lies closest to θ_j, otherwise $u_{ij} = 0$ [22].

Initially, arbitrary positions of the k prototypes or centroids are assigned beforehand. Afterwards, each member of the dataset $X = \{x_1, x_2, \ldots, x_N\}$, that in this case represent all pairs of EEG channel phase differences in a specific frequency band, is designated to a class according to the nearest neighbourhood allocation. Each group's prototype is then updated by adjusting it to the mean of the samples assigned to that particular group on the previous step. This process is repeated iteratively until the data vectors from the dataset X form compact clustering, meaning there is no significant change in the prototypes within two successive iterations [23]. Table 1 shows a summary of the steps followed to determine the right number of synchrostates.

An accurate estimation of the number of clusters is crucial to obtain reliable results. To this end the algorithm is run within a predefined range of clusters, ranging between 2 and 10 [24]. For each one of these cluster numbers the minimum value of the cost function is saved ($J = \{J_2, J_3, J_4, \ldots, J_{10}\}$) as indicated in Table 1. Plotting the cost function values J against the number of clusters (ranging from 2 to 10) the optimal number of clusters can be selected where a significant local change, a minimum, is observed. The absence of local changes indicates that there is no clustering structure underlying the dataset. Accordingly, due to the intrinsic nature of this iterative method it is possible that there is more than one significant change in the graph. In this case, the earliest one will be considered as the optimal number of clusters [19,22].

In the same manner and due to its definition, the *k*-means algorithm cannot guarantee the achievement of a global minimum of the cost function (θ, U); returning instead, clusters corresponding to local minima of the cost function. To optimize the process, and to avoid the local minima problem [19,22], a number of random initializations are run for each one of the number of clusters previously chosen (ranging from 2 to 10 as a wide representation of possible optimal number of clusters), selecting the minimum value of J for each case. In the present paper, the number of random initializations were set to 10, after trying with 50 and 100 random initializations. The increment of the number of initializations led to the same optimal number of clusters with a considerably higher computational cost, therefore the number of initializations were set at 10 which is consistent with previous literature [19].

Once the phase difference-based clusters have been identified for each condition (*Thinking R* and *Thinking* L), their temporal stability needs to be quantified. This is because the clustering algorithm cannot provide information relative to a how long the stability of each one of the unique clusters lasts. This can be done by means of synchronization index $\gamma_{xy}(b)$ which is an inverse circular statistical analogue of variance [9,12] as explained in Eq. (3).

$$\gamma_{xy}(b) = \frac{1}{N}\left(\left[\sum_t \cos\Delta\emptyset_{xy}^b(t)\right]^2 + \left[\sum_t \sin\Delta\emptyset_{xy}^b(t)\right]^2\right), \tag{3}$$

where N is the number of time points associated with a single state and b the frequency band of interest. This synchronization index lies in the interval [0,1]. When the distribution of the phase differences in widely distributed, the time average of both trigonometric function of Eq. (3) are zero indicating a small value of synchronization index. By contrast, higher values of $\gamma_{xy}(b)$ indicates that phase differences between the two processes in this particular frequency band b are in synchrony representing a low variation along time [9].

3.3. Brain connectivity metrics

The matrix containing the synchrony indices, calculated for each one of the clusters previously obtained, can be used as an adjacency matrix to determine a complex network. This network that can lead to a more quantitative description of the information coupling. Consistent with graph theory, functional brain networks can be described as graphs that are composed of nodes (EEG electrodes) which are linked by edges representing physical connections (in this particular case the values of $\gamma_{xy}(b)$) [9,21]. In the present study, the synchronization index is used to define a weighted network. Afterwards, this network is thresholded, preserving the strongest 5% of the edges or links. Fixing the density of the network is a necessary step to can compare the networks and their features across different conditions [25].

Core measures of graph theory referring to the concepts of brain integration and segregation have been employed to determine the brain connectivity under different situations, especially in studies regarding face perception in autistic populations [19]. Networks can be characterized at different levels ranging from properties explaining the whole network at the global scale to properties of network components at a local scale. The networks measured and used throughout this study can be divided into individual network measures, measures of functional segregation (measuring the

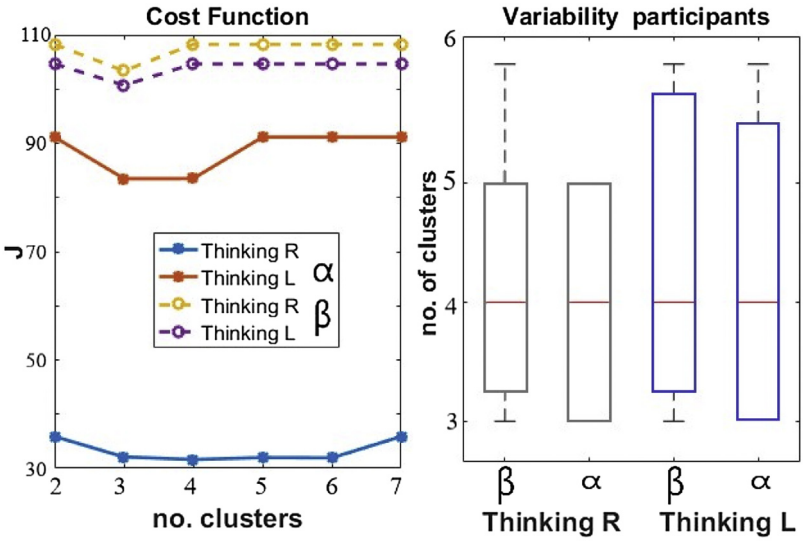

Fig. 2. Clustering results. Left graph shows the cost function to determine the optimal number of clusters k for an averaged population. Results are illustrated for the α band (solid lines) and the β band (dotted lines) for the two MI tasks used in this study: 'Thinking R' (top and bottom lines) and 'Thinking L' (the two middle lines). It can be seen that the optimal number of clusters for all cases in set 3 following the "first knee" criterion. The right-hand graph depicts the variation of the optimal number of clusters across participants all the cases under study.

ability of specialized processing) and functional integration (ability to rapidly combine specialized information from distributed brain regions) [26]. Further explanations of these complex brain networks can be found in the tutorial about connectome analysis develop by Kaiser [27]. Mathematical definitions for binary and weighted network metrics can be found in reviews provided by Rubinov and Bullmore [26,28].

The individual network metrics selected for this study were the highest degree and the mean strength. We selected the highest degree and not the mean degree as we have predefined the density of the network with the thresholding step, so the highest degree will give us more information. As measures of functional segregation, we selected transitivity (T), modularity (Q) and local efficiency (LE). Finally, within the group of functional integration measures we selected characteristic path length (CPL) and global efficiency (GE). This will give us a wide scope of the different aspect of the networks and which possible metrics are the most suitable to use to differentiate between conditions.

4. Results

The EEG data was collected from ten participants as described in Section 2. Recordings were referenced online with the average of the left and right earlobe electrodes, filtered with a notch filter (50 Hz) and a Butterworth band pass filter (0.5–100 Hz). The complete dataset was visually inspected to eliminate those trials with artifacts, baseline corrected and divided into epochs for the two task conditions, *Thinking R* and *Thinking L*. The epoch duration was 1 s, from 100 ms pre-stimulus to 900 ms post-stimulus. The instantaneous phase difference between all pairs of electrodes was computed following the algorithm described in Section 3. As a result, a series of symmetric square matrices with main diagonal elements set to zero were obtained for each particular time instant, trial, frequency band, participant and condition.

4.1. Clustering results

In order to select the optimal number of states underlying the dataset the incremental *k-means* algorithm was run for a number of clusters ranging from 2 to 10 as explained in Section 3.2. The result for each one of the frequency bands and task conditions is illustrated in Figure Fig. 2.

The graph on the left of Fig. 2 illustrates the estimation of the optimal k for each one of the frequency bands and task conditions. As mentioned in Section 3.2, the selection of the optimal k will be the first one achieving a minimum of the cost function, usually named "knee". Following this selection criterion, the number of optimal clusters for the α and β bands is $k=3$. In the case of the α band it can be argued that the algorithm achieved a stable minimum at $k=4$. In cases were multiples "knees" are present, the earliest and most prominent knee is the method conventionally used in machine learning as it explains the dataset with a minimum complexity [19]. Consequently, following this criterion, $k=3$ is the selected number for all frequency bands and conditions.

On the right side of Fig. 2 can be seen the variation of the number of synchrostates across participants for both tasks and frequency bands under consideration. The small variation of the number of optimal clusters, between 3 and 6, indicates that it is highly dependent for each individual person. It may be also indicative of other background processes occurring simultaneously to the MI task that can be reflected in the final results of the clustering step.

Once the optimal number of clusters have been decided for each condition, we plotted the transitions between the selected number of states for each time instant. Figs. 3 and 4 represent this switching pattern among states for the α and β bands respectively. The two red vertical lines in each individual plot represent the time instant when the stimulus is presented on the screen and when it disappeared respectively. Interestingly, in both frequency bands the patterns are completely different for both conditions. This may reflect that the sequence and duration of each state is task-specific. Indicating that the study of these quasi-stable states can be an effective tool for quantitative characterize the information processing ability of the brain [29,30].

For both conditions in the α band (Fig. 3) there is only one state during pre-stimulus period. Similarly, during the post-stimulus or thinking time period there is also no transitions in either conditions. On the other hand, the 500 ms corresponding to the presence of the stimulus on the screen contains a considerable number of transitions between the different states for both MI tasks. It can be interpreted that the entrance of the schematic faces on the screen triggers the nervous system to establish the necessary connections

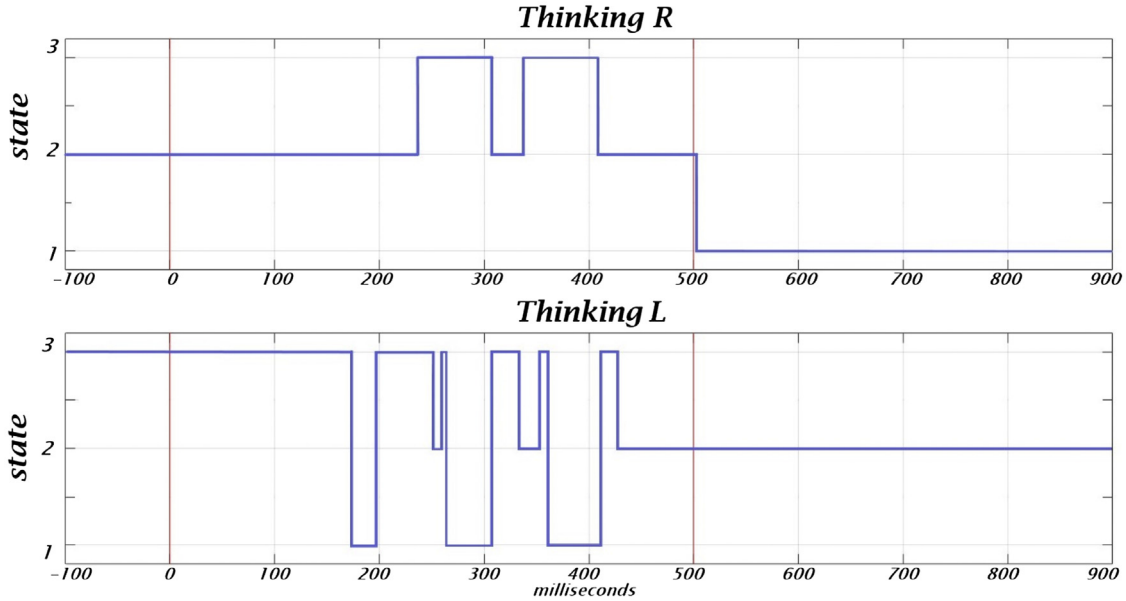

Fig. 3. Temporal evolution of the clustered synchrostates for the α band for both conditions; Thinking R (top) and Thinking L (bottom). The vertical red lines indicate the time instants of the stimulus onset and offset respectively. (For interpretation of the references to colour in this figure legend, the reader is referred to the web version of this article.)

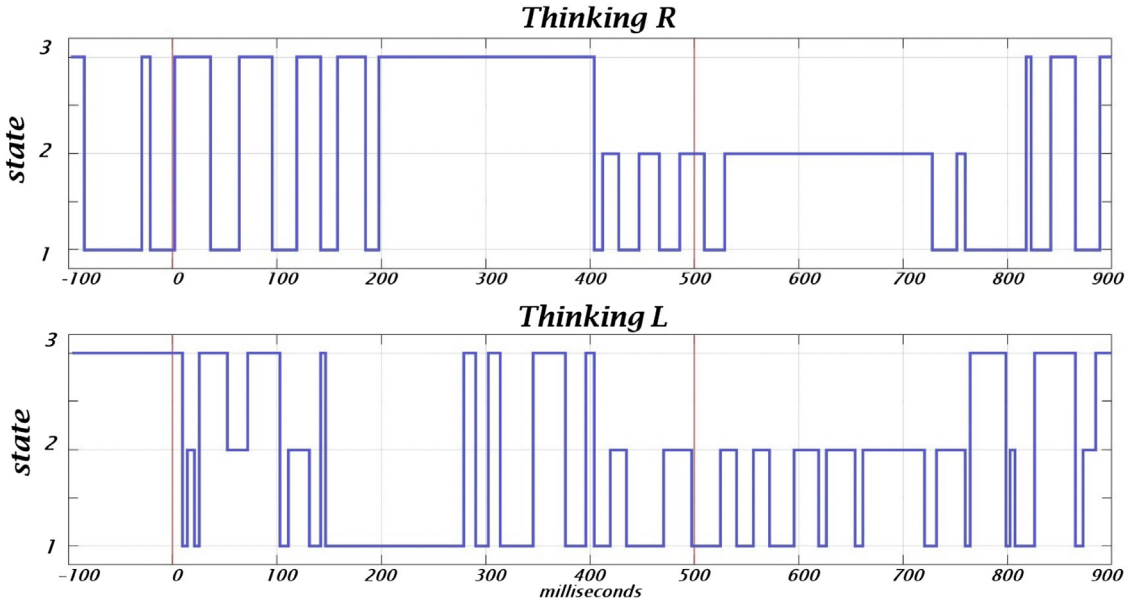

Fig. 4. Temporal evolution of the clustered synchrostates for the β band for both conditions; Thinking R (top) and Thinking L (bottom). The vertical red lines indicate the time instants of the stimulus onset and offset respectively. (For interpretation of the references to colour in this figure legend, the reader is referred to the web version of this article.)

across the brain to firstly identify the corresponding hand (left or right) and posteriorly to start thinking on the linked imagery movement.

The transitions across time between the different synchrostates for the β band is shown in Fig. 4. At first glance it can be seen that the number of transitions for both conditions is larger than in the α band. These differences between frequency bands and between conditions within a frequency band demonstrates the task-specific nature of these synchrostates [19].

From Figs. 3 and 4 can be seen than some states occur more often than others. In order to study the consistence of the synchrostates for each condition and frequency band, the number of time instants each one of states occurs is calculated. A summary of the results is shown in Table 2. Additionally, the number of transitions between states is also presented in the last column of the table for each case. It is noticeable that the number of transitions between states is larger for *Thinking L* condition than *Thinking R*. It can be thought that *Thinking L* condition is a more complex task for the participants as all of them, except one, are right handed but a study with a larger number of participants should be done to can obtain conclusive results.

Additionally, the centroid points from the selected number of clusters k, are used to generate a head plot topography. This will graphically illustrate how the electrodes having a similar difference of phase are connected across different brain regions. The values are normalized between 0 and 1 for visualization purposes. Where val-

Table 2
Number of occurrences for each one the three synchrostates for the α band (left column) and the β band (right column) with two different conditions, Thinking R (top row) and Thinking L (bottom row). The last column for each frequency band indicates the number of switches between the three synchrostates along the time duration of the epoch.

	α band				β band			
	state 1	state 2	state 3	no. transitions	state 1	state 2	state 3	no. transitions
Thinking R	103	107	46	**6**	89	68	99	**29**
Thinking L	30	129	97	**12**	103	70	83	**44**

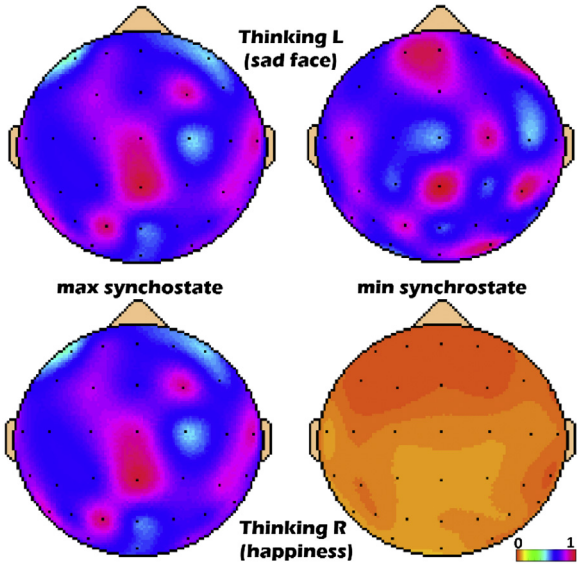

Fig. 5. Maximum (max) and minimum (min) number of occurrences synchrostates topographies for the α band. The head-plots are illustrated for the two different MI-tasks: Thinking L (first row) and Thinking L (second row).

ues near to 1 (reddish colours) mean a higher phase difference of this electrode with respect to the rest of the electrodes. By contrast, lower values (closer to 0, oranges colours), indicate that the electrode has smaller phase difference with the rest of the electrodes. Fig. 5 shows the contour plots for the α band for the maximum (*max*) and minimum (*min*) number of occurrences synchrostates for both conditions (*Thinking R* and *Thinking L*) within the length of the considered epoch for the averaged population. The selection only of max and min synchrostates is not arbitrary, due to the fact that the optimal number of the states coming from the clustering process varies among participants the criterion followed to further analyse the data is considering only these two synchrostates for each participant to can compare across them and between conditions [29,30].

Furthermore, the min synchrostate for the *Thinking R* condition (bottom right corner) presents an almost constant distribution across the whole set of electrodes, this is not related to a lack of activity. It may be due to the type of information, more uniformly distributed, occurring during these states across the brain regions. Note that the head-plots from Fig. 5 are not the standard topographies representing the spectral power over the scalp, they concept is completely different. They give an idea of the averaged phase difference distribution over the scalp during each MI task.

4.2. Brain connectivity metrics results

The synchronization index measures can be used to translate the information given by the synchrostates into complex measures giving an idea of how well connected each pair of nodes are and furthermore, about the temporal stability of the connection or synchronization. The network measures and connectivity graphs are computed using the grand average across all participants and individually. As explained in Section 3.3, 62 EEG electrodes are used as nodes and the synchronization index given by Eq. (3) as an adjacency matrix (weighted edges). All the network graphics and measures are computed using EEGNET and BCT toolboxes [26,32]. Table 3 shows a summary with all the network measures resulting from the grand average analysis, after a 5% threshold is applied, for the α and the β bands respectively.

These connectivity metrics were obtained for each participant to can perform a more detailed statistical analysis, always having in account the reduced number of participants for this study. To check for this issue, different metrics for effect size are also calculated within the statistical analysis. Hedges'g for paired *t*-test and η^2 for two-ways Anova were selected to this end.

Due the small difference in the optimal number of synchrostates only the *max* and *min* states are selected from each participant in order to can perform a comparison. For each frequency band a paired *t*-test was performed to compare *max* and *min* states for each condition (*Thinking R* and *Thinking L*) and a 2-ways ANOVA was also performed to compare the state (*max*/*min*) and condition for each frequency band.

Results for the α band *Thinking R* condition only showed significant differences for the highest degree ($t = 2.82$, $p = 0.01$, Hedges'g=1.20) and mean Strength ($t = 2.83$, $p = 0.01$, Hedges'g=1.21) when comparing the *max* and *min* states. The rest of the metrics under consideration had *p* values over 0.5. On the other hand, when comparing *max* and *min* states for the *Thinking* L condition no significant differences were found for any connectivity metrics. The lowest value corresponded to the LE with $t = 0.86$, $p = 0.39$, Hedges'g=0.37. Finally, when comparing state and condition, statistically significant differences were found for *Thinking R* versus *Thinking L* for LE ($F = 5.29$, $p = 0.04$, $\eta^2 = 0.02$) and a trend for highest degree ($F = 3.40$, $p = 0.09$, $\eta^2 = 0.08$) and strength ($F = 3.40$, $p = 0.09$, $\eta^2 = 0.07$). Furthermore, a trend in the interaction effect between state and condition was found for degree ($F = 3.71$, $p = 0.08$, $\eta^2 = 0.05$) and strength ($F = 3.70$, $p = 0.08$, $\eta^2 = 0.05$).

On the other hand, no significant effects were detected for β band for *max* and *min* states within any of the conditions (lowest *p* value for *Thinking R* condition was 0.23 and 0.52 for *Thinking L* condition). Results for the two-ways analysis, including state and condition, detected for transitivity a trend within state ($F = 3.53$, $p = 0.09$, $\eta^2 = 0.03$), nothing for condition ($F = 0.44$, $p = 0.52$, $\eta^2 = 0.01$) but a significant interaction effect ($F = 7.60$, $p = 0.08$, $\eta^2 = 0.08$).

However, these results can only be understood as an indicative of a possible effect but due to the small sample size no further conclusions can be obtained. Despite of the fact that the statistically there is no many differences, the connectivity metrics obtained from the synchrostates are able to classify between the two different tasks (left and right hand) when more complex mechanisms, such as machine learning, are used as we had demonstrated in [30].

5. Discussion

The phenomenon of synchrostates, understood as a small number of unique identifiable patterns by means of phase synchrony,

Table 3
Network metrics for each one of the synchrostates for both conditions, Thinking R and Thinking L in the α band (left, white background) and β band (right, greyish background) from the grand averaged. The graph metrics used are characteristic path length (CPL), global efficiency (GE), local efficiency (LE), highest degree, mean strength, modularity (Q) and transitivity (T).

Metric	α band						β band					
	Thinking R			Thinking L			Thinking R			Thinking L		
	State 1	State 2	State 3	State 1	State 2	State 3	State 1	State 2	State 3	State 1	State 2	State 3
CPL	4.45	3.39	4.35	4.01	3.26	3.36	4.40	4.33	4.35	4.41	4.21	3.80
GE	0.14	0.08	0.14	0.12	0.10	0.11	0.14	0.14	0.14	0.12	0.16	0.13
LE	0.10	0.19	0.18	0.29	0.23	0.27	0.27	0.31	0.29	0.34	0.27	0.33
Degree	9	7	11	7	11	9	12	9	9	8	7	9
Strength	11.9	9.99	13.9	10.9	12.9	7.99	9.98	10.9	10.9	9.99	10.9	10.9
Q	0.69	0.64	0.68	0.65	0.57	0.57	0.63	0.67	0.70	0.69	0.69	0.64
T	0.82	0.74	0.70	0.79	0.62	0.64	0.71	0.80	0.80	0.86	0.80	0.75

have been shown to exist in MI tasks using schematic faces as stimuli. From the results it can be seen that these synchrostates described differentiable transition models accordingly to the stimuli presented to the participant, modelling the brain activity dynamics based on specific tasks.

In this study we demonstrated that these synchrostates are stable at a group level as individually with a minimum variation in the number of selected clusters. Furthermore, the phenomena of synchrostates has also been studied in a reduced of number of trials (50 trials, 20 trials and 10 trials) in [9], showing that the number of states obtained was independent of how the data was divided. However, a more exhaustive study with a large cohort of participants should be performed to determine the existence of these states in single trials. This will allow the possibility of using this protocol for online motor imagery based BCI applications.

The temporal dynamic of the phase synchronization is studied here by means of unsupervised pattern recognition techniques to identify the synchrostates. This idea is similar to the well stablish existence of microstates, were the clustering is done based on power amplitude instead of phase synchrony [2]. Hence, the representation of the topographies in this document are not the widely used averaged power spectrum scalp plots. In this case, large concentration of phase differences should not be confused with possible artifacts. Synchrostates resolution is in the order of milliseconds, in contrast artifacts appear in time in the order of seconds [9]. In addition, muscle artifacts are demonstrated to be more prominent at higher frequencies over 60 Hz and the results obtained are reported for β and α band so are less likely to be affected by muscle movements [31].

It can be argued that connectivity measures among EEG channels can be affected by volume conduction effect even if all brain sources are independent [32]. To avoid this problem some connectivity measures have been developed which are robust to volume conduction interference, consequently their significant connectivity estimations are only indicators of the brain interactions [33]. Some of these connectivity measures are: phase lag index (PLI) [34], the imaginary part of coherence (Imc) [35], weighted PLV or weighted PLI [33,36]. The present work on phase synchrony can be seen as an extension of this robust measures of EEG-based connectivity, subsequently the same arguments can be used to validate that the synchrostates phenomena are not under the effect of volume conduction.

6. Conclusion

The main finding of the proposed method is the identification of unique and consistent synchrostates along different frequency bands during motor imagery tasks. These synchrostates may be interpreted as the different sub-tasks, if ever possible, that the brain performs to develop an answer to a specific stimulus. Furthermore, the temporal evolution of the switching pattern of these synchrostates has also been studied. The results show that these patterns are stimuli dependent and markedly different between the two motor imagery tasks under consideration in this study. Hence, this methodology is able to classify clearly between both conditions and consequently can potentially be used in brain computer interface applications among others.

Translating these findings into graph theory complex networks to measure more quantitatively the differences between synchrostates and conditions, additionally to their temporal stability, has resulted in an efficient mechanism to understand better the underlying mechanisms of the brain when a specific task is being performed. Brain connectivity metrics form the synchrostates not only can be used to obtain a deeper understanding of the brain processing mechanism but also as features for classification using machine learning as we demonstrated in [30]. Using typical classification algorithms as linear discriminant analysis and support vector machine we obtained accuracies over 90% for left-right discrimination task. However, this process was performed across subjects. Further efforts will be addressed towards the study of synchrostates in single trials to develop an online-MI BCI system.

This work is based on the use of emotional faces or emoticons as stimuli, nevertheless more studies should be undertaken to be assured that the synchrostates phenomena is also present using other types of tasks or stimuli. Furthermore, a more standardized classification method in BCI studies, for instance common spatial patterns, should be used to determine the effectiveness of using faces showing emotions as stimuli for MI based BCI applications.

Declaration of Competing Interest

All authors have participated in (a) conception and design, or analysis and interpretation of the data; (b) drafting the article or revising it critically for important intellectual content; and (c) approval of the final version.

This manuscript has not been submitted to, nor is under review at, another journal or other publishing venue.

Acknowledgment

We would like thank Dr. Saptarshi and Dr. Valentina Bono from the University of Southampton for their inestimable help and support.

Appendix A. Supplementary data

Supplementary material related to this article can be found, in the online version, at doi:https://doi.org/10.1016/j.bspc.2019.101630.

References

[1] A.M. Bastos, J.-M. Schoffelen, A tutorial review of functional connectivity analysis methods and their interpretational pitfalls, Front. Syst. Neurosci. (2016).
[2] C.-F. Lu, et al., Reorganization of functional connectivity during the motor task using EEG time-frequency cross mutual information analysis, Clin. Neurophysiol. 122 (2011) 1569–1579.
[3] A. Almurshedi, A.K. Ismail, Cross coherence independent component analysis in resting and action states EEG discrimination, J. Phys. Conf. Ser. (2014).
[4] M. Gongora, B. Velasques, M. Cagy, S. Teixeira, P. Ribeiro, EEG coherence as a diagnostic tool to measure the initial stages of Parkinson Disease, Med. Hypotheses (2019).
[5] L. Leocani, C. Toro, P. Manganotti, P. Zhuang, M. Hallett, Event-related coherence and event-related desynchronization/synchronization in the 10 Hz and 20 Hz EEG during self- paced movements, Electroencephalogr. Clin. Neurophysiol. - Evoked Potentials 104 (3) (1997) 199–206.
[6] J. Bendat, A. Piersol, Engineering Applications of Correlation and Spectral Analysis, 1993.
[7] F.J. Varela, J.-P. Lachaux, E. Rodriguez, J. Martinerie, The brainweb: phase synchronization and large-scale integration, Nat. Rev. Neurosci. 2 (4) (2001) 229–239.
[8] R.Q. Quiroga, A. Kraskov, T. Kreuz, P. Grassberger, Performance of different synchronization measures in real data: a case study on electroencephalographic signals, Phys. Rev. E - Stat. Nonlinear, Soft Matter Phys. 65 (4) (2002).
[9] W. Jamal, S. Das, K. Maharatna, I. Pan, D. Kuyucu, Brain connectivity analysis from EEG signals using stable phase-synchronized states during face perception tasks, Phys. A Stat. Mech. Appl. 434 (2015) 273–295.
[10] S. Liang, K.-S. Choi, J. Qin, Q. Wang, W.-M. Pang, P.-A. Heng, Discrimination of motor imagery tasks via information flow pattern of brain connectivity, Technol. Health Care 24 (June (s2)) (2016) S795–S801.
[11] M. Grosse-Wentrup, Understanding brain connectivity patterns during motor imagery for brain-computer interfacing, Adv. Neural Inf. Process. Syst. 21 (2008) 561–568.
[12] K. Nishida, et al., EEG microstates associated with salience and frontoparietal networks in frontotemporal dementia, schizophrenia and Alzheimer's disease, Clin. Neurophysiol. 124 (6) (2013) 1106–1114.
[13] F. Musso, J. Brinkmeyer, A. Mobascher, T. Warbrick, G. Winterer, Spontaneous brain activity and EEG microstates. A novel EEG/fMRI analysis approach to explore resting-state networks, Neuroimage 52 (4) (2010) 1149–1161.
[14] S. Cacioppo, S. Balogh, J.T. Cacioppo, Implicit attention to negative social, in contrast to nonsocial, words in the stroop task differs between individuals high and low in loneliness: evidence from event-related brain microstates, Cortex 70 (2015) 213–233.
[15] C. Andreou, et al., Resting-state connectivity in the prodromal phase of schizophrenia: insights from EEG microstates, Schizophr. Res. 152 (2–3) (2014) 513–520.
[16] Y. Zhang, Q. Zhao, J. Jing, X. Wang, A. Cichocki, A novel BCI based on ERP components sensitive to configural processing of human faces, J. Neural Eng. 9 (2) (2012), 026018.
[17] L. Santamaria, C. James, Use of graph metrics to classify motor imagery based BCI, in: 2016 International Conference for Students on Applied Engineering (ISCAE), 2016, pp. 469–474.
[18] g.tec medical engineering, "g.Tec: medical engineering." [Online]. Available: www.gtec.at. (Accessed 01 January 2014).
[19] W. Jamal, et al., On the existence of synchrostates in multichannel EEG signals during face-perception tasks, Phys. Eng. Express 1 (1) (2015), 15002.
[20] R.D. Bickford, Electroencephalography, in: Enclyclopedia of Neuroscience, Birkhauser Verlag AG, Cambridge (USA), 1987, pp. 371–373.
[21] A.K. Jain, B. Chandrasekaran, Dimensionality and sample size considerations in pattern recognition practice, Handb. Stat. 2 (May) (1982) 835–855.
[22] S. Theodoridis, A. Pikrakis, K. Koutoumbas, D. Cavouras, Introduction to Pattern Rcognition, a Matlan Approach, Academic Press, United States, 2010.
[23] M. Kyan, P. Muneesawang, K. Jarrah, L. Guan, Unsupervised Learning: A Dyanmic Approach, John Wiley & Son, Inc., New Jersey (USA), 2014.
[24] W. Jamal, Investigating Phase Synchronisation in EEG Signals for Brain Connectivity Analysis, 2014.
[25] J. Toppi, et al., Investigating cooperative behavior in ecological settings: an EEG hyperscanning study, PLoS One 11 (4) (2016) 1–26.
[26] M. Rubinov, O. Sporns, Complex network measure of brain connectivity: uses and interpretations, Neuroimage 52 (2010) 1059–1069.
[27] M. Kaiser, A tutorial in connectome analysis: topological and spatial features of brain networks, NeuroImage 57 (3) (2011) 892–907.
[28] E. Bullmore, O. Sporns, Complex brain networks: graph theoretical analysis of structural and functional systems, Nat. Rev. Neurosci. 10 (March (3)) (2009) 186–198.
[29] W. Jamal, S. Das, I.-A. Oprescu, K. Maharatna, F. Apicella, F. Sicca, Classification of autism spectrum disorder using supervised learning of brain connectivity measures extracted from synchrostates, J. Neural Eng. 11 (4) (2014), 046019.
[30] L. Santamaria, C. James, Using brain connectivity metrics from synchrostates to perform motor imagery classification in EEG-based BCI systems, Healthc. Technol. Lett. 5 (June (3)) (2018) 88–93.
[31] J. Ma, P. Tao, S. Bayram, V. Svetnik, Muscle artifacts in multichannel EEG: characteristics and reduction, Clin. Neurophysiol. 123 (8) (2012) 1676–1686.
[32] M. Lai, M. Demuru, A. Hillebrand, M. Fraschini, A comparison between scalp- and source-reconstructed EEG networks, Sci. Rep. (2018).
[33] A. Khadem, G.-A. Hossein-Zadeh, Quantification of the effects of volume conduction on the EEG/MEG connectivity estimates: an index of sensitivity to brain interactions, Physiol. Meas. 35 (10) (2014) 2149–2164.
[34] C.J. Stam, G. Nolte, A. Daffertshofer, Phase lag index: assessment of functional connectivity from multi channel EEG and MEG with diminished bias from common sources, Hum. Brain Mapp. 28 (11) (2007) 1178–1193.
[35] J.M. Sanchez Bornot, K.F. Wong-Lin, A.L. Ahmad, Robust EEG/MEG based functional connectivity with the envelope of the imaginary coherence: sensor space analysis, Brain Topogr. 31 (2018) 895.
[36] F. Li, T. Zhang, B.J. Li, W. Zhang, J. Zhao, L.P. Song, Motor imagery training induces changes in brain neural networks in stroke patients, Neural Regen. Res. (2018).